






Quantitative assessment of the universal thermopower in the Hubbard model

Received: 6 June 2023

Accepted: 17 October 2023

Published online: 03 November 2023

Wen O. Wang ^{1,2}✉, Jixun K. Ding ^{1,2}, Edwin W. Huang ^{3,4,5}, Brian Moritz ² & Thomas P. Devereaux ^{2,6,7}✉

As primarily an electronic observable, the room-temperature thermopower S in cuprates provides possibilities for a quantitative assessment of the Hubbard model. Using determinant quantum Monte Carlo, we demonstrate agreement between Hubbard model calculations and experimentally measured room-temperature S across multiple cuprate families, both qualitatively in terms of the doping dependence and quantitatively in terms of magnitude. We observe an upturn in S with decreasing temperatures, which possesses a slope comparable to that observed experimentally in cuprates. From our calculations, the doping at which S changes sign occurs in close proximity to a vanishing temperature dependence of the chemical potential at fixed density. Our results emphasize the importance of interaction effects in the systematic assessment of the thermopower S in cuprates.

The Hubbard model, despite decades worth of study, remains enigmatic as a model to describe strongly correlated systems. Due to the fermion sign problem and exponential complexity, only one-dimensional systems have lent themselves to error-free estimations of ground states and their properties. Recently, angle-resolved photoemission studies have demonstrated that a one-dimensional Hubbard-extended Holstein model can quantitatively reproduce spectra near the Fermi energy^{1–3}. In two dimensions, the community lacks exact results in the thermodynamic limit; nevertheless, many of the extracted properties from simulations of the Hubbard model bear a close resemblance to observables measured in experiments, particularly those performed on high-temperature superconducting cuprates. These properties include the appearance of antiferromagnetism near half-filling, stripes, and strange metal behavior^{4–6}. However, quantitative assessments have remained out of reach, particularly regarding transport properties, where multi-particle correlation functions (calculations involving the full Kubo formalism) are computationally intensive, or one must rely on single-particle quantities (i.e., Boltzmann formalism), which can be conceptually problematic for strong interactions.

In principle, the high-temperature behavior of the thermopower (thermoelectric power, or Seebeck coefficient) S offers the possibility to directly test the Hubbard model against experiments in strongly correlated materials like the cuprates. Above the Debye temperature, phonons are essentially elastic scatterers of electrons and one might expect thermal relaxation to come overwhelmingly from inelastic scattering off of other electrons. Moreover, room-temperature measurements afford direct contact with determinant quantum Monte Carlo (DQMC)^{7,8} simulations, which are limited by the fermion sign problem to temperatures above roughly $J/2$ (half of the spin-exchange energy). Thus, one can address directly an essential question—can the Hubbard model give both qualitative and quantitative agreement with the observed thermopower in cuprates at high temperatures?

Systematic studies of the room-temperature thermopower across a wide variety of cuprates^{9–17} show that the thermopower falls roughly on a universal curve over a broad range of hole doping p , with a more-or-less universal sign change near optimal doping. This sign change has been interpreted as evidence for a Lifshitz transition^{18–20}; however, this implies that the doping associated with the sign change depends

¹Department of Applied Physics, Stanford University, Stanford, CA 94305, USA. ²Stanford Institute for Materials and Energy Sciences, SLAC National Accelerator Laboratory, 2575 Sand Hill Road, Menlo Park, CA 94025, USA. ³Department of Physics and Institute of Condensed Matter Theory, University of Illinois at Urbana-Champaign, Urbana, IL 61801, USA. ⁴Department of Physics and Astronomy, University of Notre Dame, Notre Dame, IN 46556, USA. ⁵Stavropoulos Center for Complex Quantum Matter, University of Notre Dame, Notre Dame, IN 46556, USA. ⁶Department of Materials Science and Engineering, Stanford University, Stanford, CA 94305, USA. ⁷Geballe Laboratory for Advanced Materials, Stanford University, Stanford, CA 94305, USA.

✉ e-mail: wenwang.physics@gmail.com; tpd@stanford.edu

on material specifics and the detailed shapes of Fermi surfaces, which is hard to reconcile with the observed universality. An alternative interpretation of the sign change appeals to the atomic limit^{21–27}; however, the atomic limit requires extremely strong interactions and a very high temperature T compared to the bandwidth, neither of which is satisfied in cuprates at room temperature. The thermopower S also has been approximated by the entropy per density, defined through the Kelvin formula $S_{\text{Kelvin}} = (\partial s/\partial n)_T/e^{28}$, where charge $e^* = -e$ for electrons. S_{Kelvin} is believed to be an accurate proxy for the thermopower S , since it accounts for the full effects of interactions, while bypassing the difficulties in exactly calculating the Kubo formula^{25,28–30}. However, a direct comparison between S and S_{Kelvin} is required before drawing any conclusions based on these assumptions.

Here, we calculate the thermopower S based on the many-body Kubo formula, as well as the Kelvin formula S_{Kelvin} , for the t - t' - U Hubbard model. We employ numerically exact DQMC and maximum entropy analytic continuation (MaxEnt)^{31,32} to obtain the DC transport coefficients that specifically enter the evaluation of S . Our results show that the Hubbard model can quantitatively capture the magnitudes and the general patterns of S that have been observed in cuprate experiments.

Results

The doping dependence of thermopower S from the Hubbard model is shown in Fig. 1 for three different sets of parameters at their lowest achievable temperatures, overlaid with experimental data from several families of cuprates. It is important to note that in the process of converting our results to real units based on universal physical quantities k_B and e , there are no adjustable parameters: S is a ratio, so the standard units of t (or U) in the Hubbard model factor out. The most striking observation is the surprisingly good agreement between our results and the room-temperature thermopower in cuprates, in both qualitative trend and quantitative magnitudes. Both the simulation and experimental data show a sign change roughly at $p \sim 0.15$. In both cases, S —a quantity proportional to the electronic resistivity—increases dramatically in the low doping regime, as the system approaches a Mott

insulator. The simulation shows moderate U and t' dependence, without significantly affecting agreement with experiments. The moderate parameter dependence is consistent with the observed approximate universality of the doping dependence of the room-temperature S for different cuprates, which may have varying effective U and t' .

For weakly interacting electrons, S is expected to change sign around the Lifshitz transition. The sign change in our model with strong interactions, which occurs at $p \sim 0.15$ for $t'/t = -0.25$, is much lower than the Lifshitz transition, which occurs at $p \sim 0.26$ for the same parameters, nor is it associated with the atomic limit (see Supplementary Note 3 and Supplementary Note 5 for details). Therefore, we seek a deeper understanding from $S_{\text{Kelvin}} = -(\partial s/\partial n)_T/e$, entropy variation per density variation at a fixed temperature, or equivalently, by the Maxwell relation, $(\partial\mu/\partial T)_n/e$, chemical potential variation per temperature variation at fixed density (see Supplementary Note 4). In Fig. 2, we compare the doping dependence of S and S_{Kelvin} . Despite differences in exact values, the sign change of S , as shown in Fig. 2a, is closely associated with that of S_{Kelvin} , as shown in Fig. 2b. The sign change of S_{Kelvin} occurs when the temperature dependence of the chemical potential μ vanishes at fixed density—an “isosbestic” point, as exemplified in the inset of Fig. 2b, and highlighted by the arrows.

The doping dependence of S and S_{Kelvin} are also qualitatively similar, and U generally affects both S and S_{Kelvin} in a similar manner, moderately reducing the doping at which each changes sign as U increases. However, t' has more significant and opposite effects on S and S_{Kelvin} . Comparing Fig. 2a and b shows us that even though S_{Kelvin} , a thermodynamic quantity, differs from S , since it does not reflect the dynamics captured by transport³³, S_{Kelvin} still reflects the most important effects from the Hubbard interaction, showing a doping dependence and sign change similar to S .

We now examine the temperature dependence of S and S_{Kelvin} , using $U/t = 6$ and $t'/t = -0.25$, shown in Fig. 3, as a representative example. The temperature dependence of S in Fig. 3a and S_{Kelvin} in Fig. 3b are qualitatively similar. As temperature decreases from high temperatures, S and S_{Kelvin} first increase, following the atomic limit ($t, t' \ll k_B T, U$, see Supplementary Note 5). As temperature decreases further and passes the scale t/k_B , their behaviors deviate from the atomic limit. At low doping ($p \lesssim 0.07$), S and S_{Kelvin} monotonically increase, but at higher doping levels, they first decrease before increasing again down to the lowest temperature, with a dip appearing in between.

We find the dip and the low-temperature increase in both S and S_{Kelvin} particularly interesting, since this upturn commonly appears in cuprates^{9–11,13,16}, and cannot be understood in either the atomic or weakly interacting limits. To understand its origin, we consider the relationship between S_{Kelvin} and the specific heat c_v using the Maxwell relation $-e(\partial S_{\text{Kelvin}}/\partial T)_p = -(\partial c_v/\partial p)_T/T$, where, by definition, $S_{\text{Kelvin}} = (\partial s/\partial p)_T/e$ and $c_v = T(\partial s/\partial T)_p$. Specific heat c_v results, also for $U/t = 6$ and $t'/t = -0.25$, are shown in the inset of Fig. 3b. Near half-filling and for temperatures below the spin-exchange energy $J (=4t^2/U$ to leading order), c_v starts to increase with decreasing temperatures, which is believed to be associated with spin fluctuations^{34–36}, and c_v drops with increasing doping. Correspondingly, S_{Kelvin} at fixed doping increases with decreasing temperatures, leading to a low-temperature upturn. As the upturn is a common feature shared by S and S_{Kelvin} , it is reasonable to believe that the origin should be the same.

The low-temperature slope of the thermopower can be compared with experiments. The negative slopes quoted in ref. 11 for $\text{Bi}_2\text{Sr}_2\text{CaCu}_2\text{O}_{8+\delta}$ and $\text{Tl}_2\text{Ba}_2\text{CuO}_{6+\delta}$ range roughly from -0.05 to $-0.02 \mu\text{V}/\text{K}^2$. Assuming $t/k_B \sim 4000 \text{ K}$, this range corresponds to $[-2.3, -0.9] k_B^2/(te)$ in our model. We estimate the slope in our model by taking the finite difference between temperatures $k_B T = t/4$ and $t/3.5$ in Fig. 3a and b. For doping between $p = 0.1$ and 0.2 , the calculated slope ranges between $[-2.1, -1.5] k_B^2/(te)$ for S , and $[-1.8, -0.2] k_B^2/(te)$ for S_{Kelvin} . Even though systematic and statistical errors in S introduce

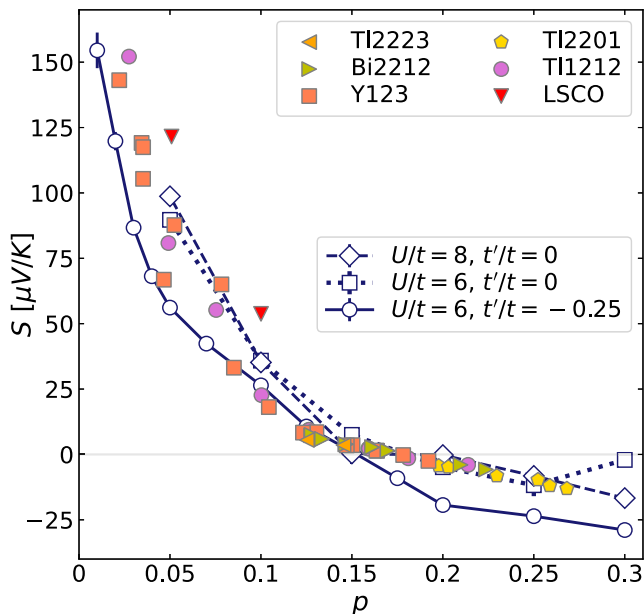


Fig. 1 | Comparison of simulated and experimental thermopower. Thermopower S as a function of doping p from DQMC simulations (empty markers connected by lines), compared with doping dependence of S for various cuprates at $T = 290 \text{ K}$ (solid scattered markers, data from refs. 9,11). For $U/t = 8$ and $t'/t = 0$, the temperature is $k_B T = t/3.5$. For $U/t = 6$, the temperature is $k_B T = t/4$ for both $t'/t = 0$ and $t'/t = -0.25$.

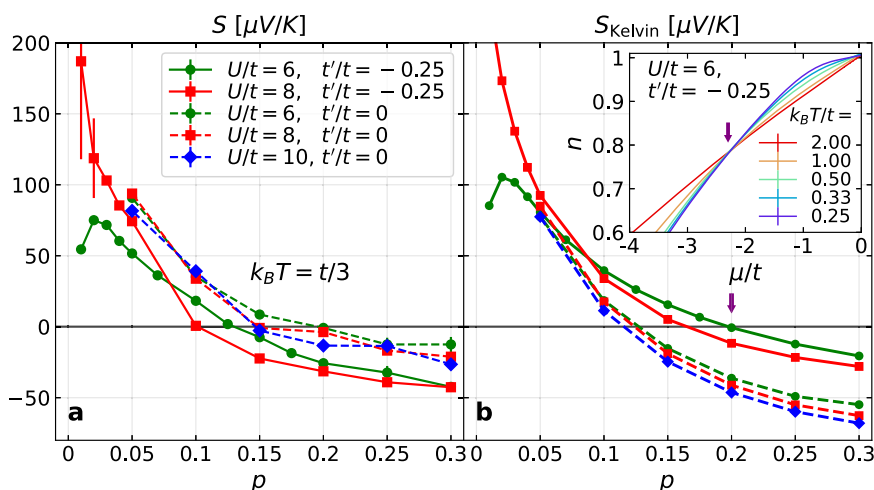


Fig. 2 | Doping dependence and sign change of S and S_{Kelvin} . Thermopower S (a) and the Kelvin formula for the thermopower S_{Kelvin} (b) as a function of doping p for the Hubbard model with different U and t' , all at the same temperature $k_B T = t/3$. Inset of (b): density n , measured using DQMC, as a function of the chemical

potential μ for $U/t = 6$, and $t'/t = -0.25$ at different temperatures T . The arrows in (b) and its inset indicate the correspondence between the sign change of S_{Kelvin} and the vanishing of the temperature dependence of μ at fixed density.

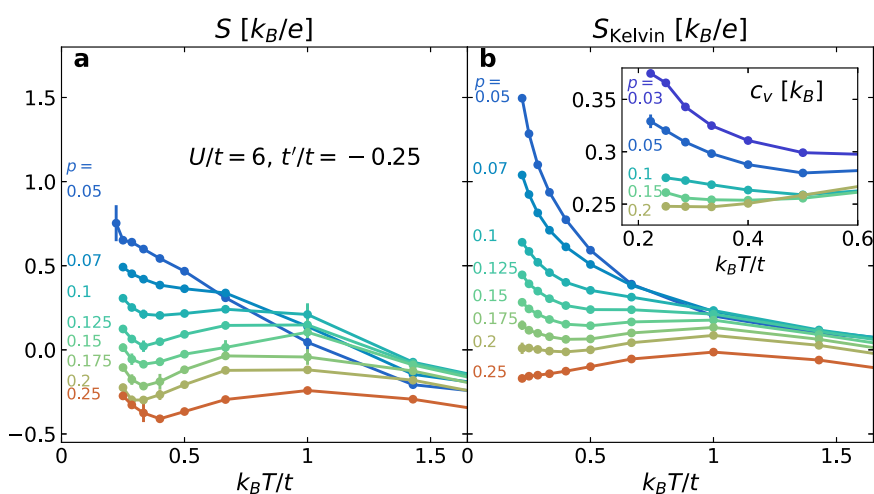


Fig. 3 | Temperature dependence of S and S_{Kelvin} . Thermopower S (a), and the Kelvin formula for the thermopower S_{Kelvin} (b), as a function of temperature T , at different doping levels p , for $U/t = 6$, and $t'/t = -0.25$. Inset of b shows the specific

heat c_v measured using DQMC as a function of temperature for different doping levels.

uncertainties to this slope estimate, the ranges are roughly comparable between simulated S , S_{Kelvin} , and experimental values.

For a detailed verification and analysis of the relationship between S_{Kelvin} and c_v , we calculate $-\partial^2 s / (\partial p \partial T)$ from derivatives of independently measured S_{Kelvin} and c_v , for both $U/t = 6$ and $U/t = 8$ with $t'/t = -0.25$, as shown in Fig. 4. Results from the two methods are consistent, up to minor discrepancies such as taking derivatives from discrete data points. At any point along the contour $\partial^2 s / (\partial p \partial T) = 0$ (black solid lines), either a peak or a dip will occur in S_{Kelvin} as a function of T . We observe that a peak appears at temperatures above J/k_B (dashed horizontal line) and a dip appears at temperatures below J/k_B . Note that $T - J/k_B$ corresponds roughly to the crossover between a peak or dip in S_{Kelvin} for both $U/t = 6$ and $U/t = 8$ (c.f. Supplementary Fig. 6), supporting our idea that the non-monotonic temperature dependence of both S_{Kelvin} and S should be associated with effects of spin exchange.

Discussion

In summary, we calculated the thermopower S and the Kelvin formula S_{Kelvin} in the Hubbard model. S shows qualitative and quantitative

agreement with the universal curve of the room-temperature S in cuprates, with a sign change corresponding to an “isosteric” point in n versus μ . S and S_{Kelvin} show qualitatively similar doping dependence, and the doping at which S changes sign corresponds well to that of S_{Kelvin} . As a function of temperature, we observe a low-temperature upturn in S and S_{Kelvin} with a slope quantitatively comparable with the corresponding linear increase in cuprates, and we provide evidence supporting their association with the scale of J . With this general agreement, we demonstrate that major features in the universal behavior of S in cuprates can be replicated through a quantitative assessment of S in the Hubbard model. The observation that S_{Kelvin} captures qualitative features of S enables us to understand the experimental thermopower results from the perspective of entropy variation with density.

We emphasize the significance of such a high level of agreement between simulations and experiments for thermopower. Transport properties can be sensitive to numerous factors, which may be different between cuprates and the t - t' - U Hubbard model. The combination of the model’s simple form and capability to reproduce

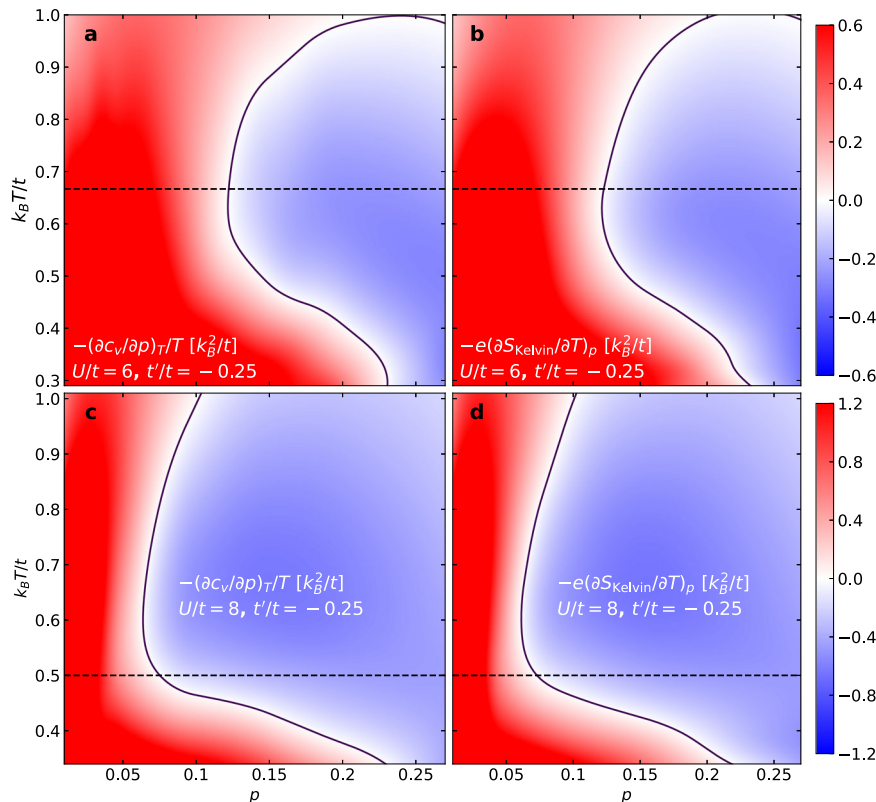


Fig. 4 | Analysis using c_v and S_{Kelvin} . Color density plots of $-\partial^2 s / (\partial p \partial T)$ calculated from doping derivative of specific heat $[-\partial c_v / \partial p]_T / T$, (**a, c**) and temperature derivative of S_{Kelvin} $[-e(\partial S_{\text{Kelvin}} / \partial T)_p]$, (**b, d**), for interaction strengths $U/t = 6$ (**a, b**) and $U/t = 8$ (**c, d**), both with $t'/t = -0.25$. A cubic-spline fit was applied to curves of c_v versus p and S_{Kelvin} versus T , with corresponding derivatives obtained from the

fits. The derivatives $-\partial^2 s / (\partial p \partial T)$ were interpolated (cubic) onto the two-dimensional (p, T) plane. Horizontal dashed lines mark the leading-order approximation for the spin-exchange energy $J = 4t^2/U$, and solid lines mark the contour where $-\partial^2 s / (\partial p \partial T) = 0$.

universal features suggests the dominance of interaction effects in the origin of the systematic behavior in the cuprates. Our observations highlight the importance of pursuing high-accuracy simulations accounting for the full effect of interactions in making progress at understanding these enigmatic materials.

Methods

We investigate the two-dimensional single-band t - t' - U Hubbard model with spin $S=1/2$ on a square lattice using DQMC^{7,8}. The Hamiltonian is

$$H = -t \sum_{\langle lm \rangle, \sigma} (c_{l,\sigma}^\dagger c_{m,\sigma} + \text{h.c.}) - t' \sum_{\langle\langle lm \rangle\rangle, \sigma} (c_{l,\sigma}^\dagger c_{m,\sigma} + \text{h.c.}) + U \sum_l \left(n_{l,\uparrow} - \frac{1}{2} \right) \left(n_{l,\downarrow} - \frac{1}{2} \right), \quad (1)$$

where t (t') is the nearest-neighbor (next-nearest-neighbor) hopping, U is the on-site Coulomb interaction, $c_{l,\sigma}^\dagger$ ($c_{l,\sigma}$) is the creation (annihilation) operator for an electron at site l with spin σ , and $n_{l,\sigma} \equiv c_{l,\sigma}^\dagger c_{l,\sigma}$ is the number operator at site l with spin σ .

The Kelvin formula for the thermopower S_{Kelvin} can be calculated using DQMC through

$$S_{\text{Kelvin}} = - \frac{\langle (H - \mu N) N \rangle - \langle H - \mu N \rangle \langle N \rangle}{eT(\langle NN \rangle - \langle N \rangle \langle N \rangle)}, \quad (2)$$

where $N = \sum_l (n_{l,\uparrow} + n_{l,\downarrow})$ is the total electron number operator, and μ is the chemical potential.

From the Hamiltonian in Eq. (1), the particle current \mathbf{J} and the energy current \mathbf{J}_E are obtained as^{37,38}

$$\mathbf{J} = \frac{t}{2} \sum_{l, \delta \in \text{NN}, \sigma} \delta (ic_{l+\delta, \sigma}^\dagger c_{l, \sigma} + \text{h.c.}) + \frac{t'}{2} \sum_{l, \delta' \in \text{NNN}, \sigma} \delta' (ic_{l+\delta', \sigma}^\dagger c_{l, \sigma} + \text{h.c.}) \quad (3)$$

and

$$\begin{aligned} \mathbf{J}_E = & \sum_{\substack{l, \delta \in \text{NN}, \\ \delta_2 \in \text{NN}, \sigma}} \left(-\frac{\delta_1 + \delta_2}{4} \right) t^2 (ic_{l+\delta_1+\delta_2, \sigma}^\dagger c_{l, \sigma} + \text{h.c.}) \\ & + \sum_{\substack{l, \delta \in \text{NN}, \\ \delta' \in \text{NNN}, \sigma}} \left(-\frac{\delta + \delta'}{2} \right) tt' (ic_{l+\delta+\delta', \sigma}^\dagger c_{l, \sigma} + \text{h.c.}) \\ & + \sum_{\substack{l, \delta_1' \in \text{NNN}, \\ \delta_2' \in \text{NNN}, \sigma}} \left(-\frac{\delta_1' + \delta_2'}{4} \right) t'^2 (ic_{l+\delta_1'+\delta_2', \sigma}^\dagger c_{l, \sigma} + \text{h.c.}) \\ & + \frac{Ut}{4} \sum_{l, \delta \in \text{NN}, \sigma} \delta (n_{l+\delta, -\sigma} + n_{l, -\sigma}) (ic_{l+\delta, \sigma}^\dagger c_{l, \sigma} + \text{h.c.}) \\ & + \frac{Ut'}{4} \sum_{\substack{l, \sigma, \\ \delta' \in \text{NNN}}} \delta' (n_{l+\delta', -\sigma} + n_{l, -\sigma}) (ic_{l+\delta', \sigma}^\dagger c_{l, \sigma} + \text{h.c.}) \\ & - \frac{Ut}{4} \sum_{l, \delta \in \text{NN}, \sigma} \delta (ic_{l+\delta, \sigma}^\dagger c_{l, \sigma} + \text{h.c.}) \\ & - \frac{Ut'}{4} \sum_{l, \delta' \in \text{NNN}, \sigma} \delta' (ic_{l+\delta', \sigma}^\dagger c_{l, \sigma} + \text{h.c.}). \end{aligned} \quad (4)$$

To make the notations above clear, NN (NNN) denotes the set of nearest-neighbor (next-nearest-neighbor) position displacements.

Specifically, on the two-dimensional square lattice, $NN = \{+\mathbf{x}, -\mathbf{x}, +\mathbf{y}, -\mathbf{y}\}$ and $NNN = \{+\mathbf{x} + \mathbf{y}, -\mathbf{x} + \mathbf{y}, +\mathbf{x} - \mathbf{y}, -\mathbf{x} - \mathbf{y}\}$, where the lattice constant is set to 1 and \mathbf{x} and \mathbf{y} are unit vectors. Here, if l is an arbitrary site label associated with the position vector $x_l\mathbf{x} + y_l\mathbf{y}$, and \mathbf{v} is a vector adding up arbitrary elements in NN and NNN , the notation $l + \mathbf{v}$ represents a unique site label associated with the position $x_{l+\mathbf{v}}\mathbf{x} + y_{l+\mathbf{v}}\mathbf{y} + \mathbf{v}$. The heat current is $\mathbf{J}_Q = \mathbf{J}_E - \mu\mathbf{J}$.

We calculate the thermopower

$$S = -\frac{L_{J_Q, J_x}}{eTL_{J_x}} \quad (5)$$

using DQMC and MaxEnt^{31,32}. Here, $J_{Q,x}$ and J_x are the x -components of the heat current operator \mathbf{J}_Q and particle current operator \mathbf{J} , respectively. For arbitrary Hermitian operators O_1 and O_2 , the DC transport coefficient $L_{O_1, O_2} \equiv L_{O_1, O_2}(\omega) \Big|_{\omega=0}$, where $L_{O_1, O_2}(\omega)$ is determined using the Kubo formula

$$L_{O_1, O_2}(\omega) = \frac{1}{N_x N_y \beta} \int_0^\infty dt e^{i(\omega + i0^+)t} \int_0^\beta d\tau \langle O_1(t - i\tau) O_2(0) \rangle, \quad (6)$$

where t is real time, without confusion with the hopping matrix elements in the Hamiltonian. Here, N_x, N_y are the sizes of the lattice along the x and y directions, respectively, $\beta \equiv (k_B T)^{-1}$, and

$$O_1(t - i\tau) = e^{i(H - \mu N)(t - i\tau)} O_1 e^{-i(H - \mu N)(t - i\tau)}. \quad (7)$$

Detailed derivations for Eqs. (5) and (2) are in Supplementary Note 2 and Supplementary Note 4, respectively. For our calculation, the units for both S and S_{Kelvin} are $k_B/e \approx 86.17 \mu\text{V/K}$.

Data availability

The data needed to reproduce the figures can be found at <https://doi.org/10.5281/zenodo.8286640>.

Code availability

The source code and analysis routines can be found at <https://doi.org/10.5281/zenodo.8286636>.

References

- Chen, Z. et al. Anomalously strong near-neighbor attraction in doped 1D cuprate chains. *Science* **373**, 1235–1239 (2021).
- Wang, Y. et al. Phonon-mediated long-range attractive interaction in one-dimensional cuprates. *Phys. Rev. Lett.* **127**, 197003 (2021).
- Tang, T., Moritz, B., Peng, C., Shen, Z.-X. & Devereaux, T. P. Traces of electron-phonon coupling in one-dimensional cuprates. *Nat. Commun.* **14**, 3129 (2023).
- Dagotto, E. Correlated electrons in high-temperature superconductors. *Rev. Mod. Phys.* **66**, 763–840 (1994).
- Arovas, D. P., Berg, E., Kivelson, S. A. & Raghu, S. The Hubbard model. *Annu. Rev. Condens. Matter Phys.* **13**, 239–274 (2022).
- Qin, M., Schäfer, T., Andergassen, S., Corboz, P. & Gull, E. The Hubbard model: a computational perspective. *Annu. Rev. Condens. Matter Phys.* **13**, 275–302 (2022).
- Blankenbecler, R., Scalapino, D. J. & Sugar, R. L. Monte Carlo calculations of coupled boson-fermion systems. i. *Phys. Rev. D.* **24**, 2278–2286 (1981).
- White, S. R. et al. Numerical study of the two-dimensional Hubbard model. *Phys. Rev. B* **40**, 506–516 (1989).
- Cooper, J. R., Alavi, B., Zhou, L.-W., Beyersmann, W. P. & Grüner, G. Thermoelectric power of some high- T_c oxides. *Phys. Rev. B* **35**, 8794–8796 (1987).
- Rao, C. N. R., Ramakrishnan, T. V. & Kumar, N. Systematics in the thermopower behaviour of several series of bismuth and thallium cuprate superconductors: An interpretation of the temperature variation and the sign of the thermopower. *Phys. C: Supercond.* **165**, 183–188 (1990).
- Obertelli, S. D., Cooper, J. R. & Tallon, J. L. Systematics in the thermoelectric power of high- T_c oxides. *Phys. Rev. B* **46**, 14928–14931 (1992).
- Tallon, J. L., Bernhard, C., Shaked, H., Hitterman, R. L. & Jorgensen, J. D. Generic superconducting phase behavior in high- T_c cuprates: T_c variation with hole concentration in $\text{YBa}_2\text{Cu}_3\text{O}_{7-\delta}$. *Phys. Rev. B* **51**, 12911–12914 (1995).
- Kaiser, A. B., Subramaniam, C. K., Ruck, B. & Paranthaman, M. Systematic thermopower behaviour in superconductors. *Synth. Met.* **71**, 1583–1584 (1995).
- Choi, M.-Y. & Kim, J. S. Thermopower of high- T_c cuprates. *Phys. Rev. B* **59**, 192–194 (1999).
- Honma, T. & Hor, P. H. Unified electronic phase diagram for hole-doped high- T_c cuprates. *Phys. Rev. B* **77**, 184520 (2008).
- Benseman, T. M., Cooper, J. R., Zentile, C. L., Lemberger, L. & Balakrishnan, G. Valency and spin states of substituent cations in $\text{Bi}_{2.15}\text{Sr}_{1.85}\text{CaCu}_2\text{O}_{8+\delta}$. *Phys. Rev. B* **84**, 144503 (2011).
- Zlatić, V., Boyd, G. R. & Freericks, J. K. Universal thermopower of bad metals. *Phys. Rev. B* **89**, 155101 (2014).
- Newns, D. M. et al. Quasiclassical transport at a van Hove singularity in cuprate superconductors. *Phys. Rev. Lett.* **73**, 1695–1698 (1994).
- McIntosh, G. C. & Kaiser, A. B. van Hove scenario and thermopower behavior of the high- T_c cuprates. *Phys. Rev. B* **54**, 12569–12575 (1996).
- Chen, K.-S. et al. Role of the van Hove singularity in the quantum criticality of the Hubbard model. *Phys. Rev. B* **84**, 245107 (2011).
- Mukerjee, S. & Moore, J. E. Doping dependence of thermopower and thermoelectricity in strongly correlated materials. *Appl. Phys. Lett.* **90**, 112107 (2007).
- Beni, G. Thermoelectric power of the narrow-band Hubbard chain at arbitrary electron density: Atomic limit. *Phys. Rev. B* **10**, 2186–2189 (1974).
- Chaikin, P. M. & Beni, G. Thermopower in the correlated hopping regime. *Phys. Rev. B* **13**, 647–651 (1976).
- Mukerjee, S. Thermopower of the Hubbard model: Effects of multiple orbitals and magnetic fields in the atomic limit. *Phys. Rev. B* **72**, 195109 (2005).
- Phillips, P., Choy, T.-P. & Leigh, R. G. Mottness in high-temperature copper-oxide superconductors. *Rep. Prog. Phys.* **72**, 036501 (2009).
- Chakraborty, S., Galanakis, D. & Phillips, P. Emergence of particle-hole symmetry near optimal doping in high-temperature copper oxide superconductors. *Phys. Rev. B* **82**, 214503 (2010).
- Mousatov, C. H., Esterlis, I. & Hartnoll, S. A. Bad metallic transport in a modified Hubbard model. *Phys. Rev. Lett.* **122**, 186601 (2019).
- Peterson, M. R. & Shastry, B. S. Kelvin formula for thermopower. *Phys. Rev. B* **82**, 195105 (2010).
- Garg, A., Shastry, B. S., Dave, K. B. & Phillips, P. Thermopower and quantum criticality in a strongly interacting system: parallels with the cuprates. *N. J. Phys.* **13**, 083032 (2011).
- Arsenault, L.-F., Shastry, B. S., Sémon, P. & Tremblay, A.-M. S. Entropy, frustration, and large thermopower of doped Mott insulators on the fcc lattice. *Phys. Rev. B* **87**, 035126 (2013).
- Jarrell, M. & Gubernatis, J. E. Bayesian inference and the analytic continuation of imaginary-time quantum Monte Carlo data. *Phys. Rep.* **269**, 133–195 (1996).
- Gunnarsson, O., Haverkort, M. W. & Sangiovanni, G. Analytical continuation of imaginary axis data for optical conductivity. *Phys. Rev. B* **82**, 165125 (2010).
- Shastry, B. S. Electrothermal transport coefficients at finite frequencies. *Rep. Prog. Phys.* **72**, 016501 (2008).
- Paiva, T., Scalettar, R. T., Huscroft, C. & McMahan, A. K. Signatures of spin and charge energy scales in the local moment and specific heat of the half-filled two-dimensional Hubbard model. *Phys. Rev. B* **63**, 125116 (2001).

35. Duffy, D. & Moreo, A. Specific heat of the two-dimensional Hubbard model. *Phys. Rev. B* **55**, 12918–12924 (1997).
36. Khatami, E. & Rigol, M. Effect of particle statistics in strongly correlated two-dimensional Hubbard models. *Phys. Rev. A* **86**, 023633 (2012).
37. Wang, W. O. et al. The Wiedemann-Franz law in doped Mott insulators without quasiparticles. *arXiv*: <https://arxiv.org/pdf/2208.09144.pdf> (2022).
38. Wang, W. O., Ding, J. K., Moritz, B., Huang, E. W. & Devereaux, T. P. Magnon heat transport in a two-dimensional Mott insulator. *Phys. Rev. B* **105**, L161103 (2022).

Acknowledgements

We acknowledge helpful discussions with D. Belitz, R. L. Greene, S. A. Kivelson, S. Raghu, B. S. Shastry, R. Scalettar, and J. Zaanen. This work at Stanford and SLAC (W.O.W., J.K.D., B.M., T.P.D.) was supported by the U.S. Department of Energy (DOE), Office of Basic Energy Sciences, Division of Materials Sciences and Engineering. E.W.H. was supported by the Gordon and Betty Moore Foundation EPiQS Initiative through the grants GBMF 4305 and GBMF 8691. Computational work was performed on the Sherlock cluster at Stanford University and on resources of the National Energy Research Scientific Computing Center, supported by the U.S. DOE, Office of Science, under Contract no. DE-AC02-05CH11231.

Author contributions

W.O.W. conceived the study, performed numerical simulations, conducted data analysis, interpreted the data, and wrote the manuscript. J.K.D., E.W.H., B.M., and T.P.D. assisted in data interpretation and contributed to writing the manuscript.

Competing interests

The authors declare no competing interests.

Additional information

Supplementary information The online version contains supplementary material available at <https://doi.org/10.1038/s41467-023-42772-8>.

Correspondence and requests for materials should be addressed to Wen O. Wang or Thomas P. Devereaux.

Peer review information *Nature Communications* thanks the anonymous reviewers for their contribution to the peer review of this work. A peer review file is available.

Reprints and permissions information is available at <http://www.nature.com/reprints>

Publisher's note Springer Nature remains neutral with regard to jurisdictional claims in published maps and institutional affiliations.

Open Access This article is licensed under a Creative Commons Attribution 4.0 International License, which permits use, sharing, adaptation, distribution and reproduction in any medium or format, as long as you give appropriate credit to the original author(s) and the source, provide a link to the Creative Commons licence, and indicate if changes were made. The images or other third party material in this article are included in the article's Creative Commons licence, unless indicated otherwise in a credit line to the material. If material is not included in the article's Creative Commons licence and your intended use is not permitted by statutory regulation or exceeds the permitted use, you will need to obtain permission directly from the copyright holder. To view a copy of this licence, visit <http://creativecommons.org/licenses/by/4.0/>.

© The Author(s) 2023